THE JOURNAL OF PHYSICAL CHEMISTRY C
A JOURNAL OF THE AMERICAN CHEMICAL SOCIETY

pubs.acs.org/JPCC

Article

Conformation-Dictated Aggregation Photophysics in Isoindigo-Based Copolymers

Published as part of The Journal of Physical Chemistry C special issue "Computational Sciences from Africa and the African Diaspora".

Eninges Asmare, Nika Bekri, Leonato Tambua Nchinda, Fekadu G. Hone, Wendimagegn Mammo, Tjaart P. J. Krüger, and Newayemedhin A. Tegegne*

Cite This: *J. Phys. Chem. C* 2024, 128, 16904−16914

Read Online

ACCESS | Metrics & More | Article Recommendations | Supporting Information

ABSTRACT: The aggregation of polymer chains directly influences the morphology of thin films used in optoelectronic devices. Therefore, understanding the relationship between the backbone conformation and aggregation of conjugated polymers is essential for ensuring optimal electronic performance. In this work, we study the effect of the backbone conformation on the aggregation photophysics of isoindigo-based copolymers, namely, bithiophene-isoindigo (**P2TI**) and thienothiophene-spaced bithiophene-isoindigo (**P2TITT**). The latter was systematically tuned by inserting thieno[3,2-*b*]thiophene (**TT**) into the former. Modification of the backbone by inserting **TT** was found to affect the planarity due to reduced steric hindrance between the donor and acceptor units. This reduced steric hindrance was further evidenced by the difference in the oscillator strength of the first excited-state transition, identified as an intramolecular charge transfer transition in time-dependent density functional theory (TD/DFT) calculations. Temperature-dependent photoluminescence (PL) of the two polymers was well reproduced using two Franck−Condon progressions, indicating the formation of both H- and J-type aggregates. This was supported by the presence of two emission lifetimes obtained from time-resolved fluorescence measurements. The evolution of the first two vibronic peaks with temperature clearly showed a stronger interchain interaction in **P2TITT**.

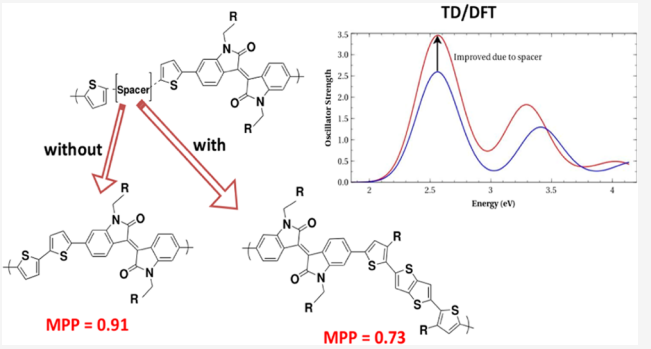

INTRODUCTION

Improving the performance of organic solar cells (OSCs) has been an active area of research for over three decades. Today, devices with power conversion efficiencies (PCEs) exceeding 19% are regularly reported, for both single-junction and multijunction devices.[1−3] This significant progress can be attributed primarily to the development of novel electron-donating and -accepting materials coupled with advancements in fabrication processes. The introduction of nonfullerene acceptors such as **Y6** has also played a crucial role in driving these efficiency advancements.[4]

Extending the absorption spectrum of the active-layer materials into the near-infrared (NIR) region enables enhanced current generation, provided the morphology of the active layer is optimized to facilitate both efficient exciton dissociation and effective charge percolation. The aggregation behavior of polymers in solution has recently gained attention in determining the formation of favorable morphologies in OSC active layers.[1,5,6] The morphology of the active layer of OSCs is determined by a combination of factors, including solvent−polymer interaction,[7] the conformation of the polymer chains,[8] and the thin film casting processes. Therefore, developing a comprehensive understanding of the relationship between the backbone conformation and aggregation behavior of conjugated polymers is essential for controlling the active-layer morphology during thin-film deposition. This, in turn, is crucial for ensuring optimal electronic performance of OSC devices.[9]

When polymer chains assemble to form aggregates, the lowest excited-state energy level can split into a doublet structure due to the $\pi-\pi$ interactions between the polymer backbones, resulting in a unique form of aggregation. In ideal H-type and J-type aggregation, the higher energy and lower energy exciton bands, respectively, correspond to the allowed electronic transitions, thereby rendering their aggregation

Received: July 18, 2024
Revised: September 17, 2024
Accepted: September 18, 2024
Published: September 26, 2024

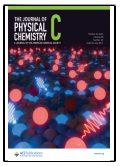

photophysics notably distinct. Few studies have demonstrated a direct correlation between the specific type of polymer aggregation and the resulting active-layer morphology, which, in turn, determines the performance of OSC devices. An interesting study by Zhao et al. revealed that the formation of H-aggregates could favor the achievement of a high open-circuit voltage, V_{OC}, while J-aggregation tends to enhance the short-circuit current, J_{SC}.[10] Another study showed that J-aggregation would be favorable for generating more excitons, as a lower energy is required to excite the J-aggregated system. In contrast, H-aggregation would tend to favor exciton dissociation by providing excitons with longer lifetimes and a stronger driving force.[11] Optimizing the solvent to control the formation of H-type and J-type aggregates in the device's active layer improved the PCE from 13.37 to 16.36%. Molecular engineering of the backbone conformation of polymers and dyes was indicated as one of the successful approaches to control the type of aggregation, whether H-type, J-type or both, within the thin films. Techniques such as modifying the side chains, molecular weight, and transition temperatures have been employed to tailor the aggregation type of polymers.[12,13] Furthermore, even minor modifications to the polymer backbone have been found to significantly impact the interchain and intrachain excitonic couplings, leading to a transition from H-like to HJ-like aggregation.[14] While structural modification of polymers has been widely used to enhance performance in OSCs, there has been little emphasis on understanding its impact on the molecular aggregation behavior. Donor−acceptor copolymers offer a unique opportunity to tailor the optical and electrical properties of polymers, especially in the context of their application in OSCs. Isoindigo has been successfully introduced as an acceptor unit in well-performing polymers. Evidently, the conformation of isoindigo-based copolymers can be controlled by the selection of the donor unit, through donor−acceptor intramolecular coupling.[15] However, to the best of our knowledge, the effect of the backbone conformation on the aggregation photophysics of isoindigo-based copolymers has not yet been reported.

In this work, we studied the effect of conformation on the aggregation photophysics of the two isoindigo-based copolymers shown in Scheme 1. The conformation of the two copolymers was systematically tuned by inserting a thieno[3,2-*b*]thiophene (**TT**) spacer in the bithiophene donor unit. This produced two copolymers, namely bithiophene-isoindigo (**P2TI**) and thienothiophene-spaced-bithiophene-isoindigo (**P2TITT**). The backbone of **P2TITT** was found to be more planar compared to **P2TI** due to reduced steric hindrance between the donor and acceptor units. Additionally, the inclusion of the **TT** unit in the donor moiety shifted the HOMO level higher owing to the stronger electron-donating ability of the **TT**-spaced donor. Franck−Condon analysis, combined with time-resolved PL, was employed to determine the aggregation type. The results indicate that the **TT**-spaced copolymer exhibits more H-type aggregation characteristics. This was further supported by temperature-dependent PL measurements showing stronger interchain interaction in **P2TITT**.

Scheme 1. Chemical Structures of the Copolymers

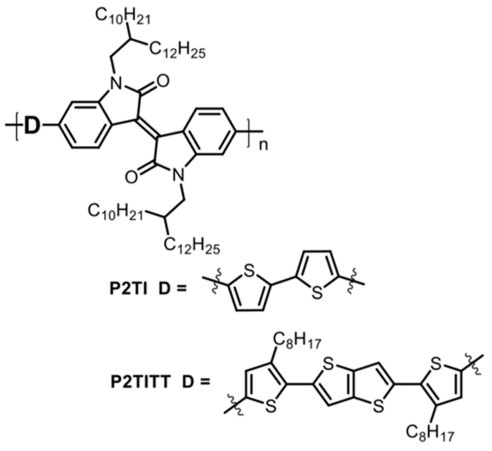

METHODS

Experimental Methods. *Optical Spectral Measurement.* The UV−vis absorption spectra of **P2TI** and **P2TITT** were measured in 1,2-dichlorobenzene (*o*-DCB) solution and as thin films using a PerkinElmer Lambda 19 UV−vis/NIR spectrophotometer. The thin films were prepared by spin-coating the polymer solutions on glass substrates at 1000 rpm, followed by annealing at 80 °C for 10 min to dry out the solvent. The PL spectra of the polymer solutions were recorded at the absorption maxima in the lower energy region using a HORIBA Jobin Yvon Fluoromax-4 spectrofluorometer. To control the temperature during the PL measurements, a Thermo Scientific NESLAB RTE-7 circulating bath was used, allowing the temperature to be varied from −5 to 85 °C.

Emission Lifetime Measurements. The emission lifetimes of the two polymers were measured in solution (0.02 mg/mL) and as thin film (15 mg/mL) using a home-built time-correlated single-photon counting (TCSPC) experimental setup, as described by Kyeyune et al.[16] The TCSPC setup was equipped with a supercontinuum picosecond pulsed laser source (SuperK EVO, NKT Photonics). An optically narrow excitation beam at 633 nm was produced by sending the laser beam through a 632.8 nm band-pass filter (FLH633-1, Thorlabs). The excitation beam was reflected by a dichroic mirror (FF649-Di01-2536 Semrock Brightline) into a water-immersion objective (Nikon CFI NIR Apochromat 60, NA 1.0). Fluorescence from the sample was measured by a single-photon avalanche diode (COUNT-T100, Laser Components) coupled to a Becker & Hickl GmbH TCSPC module (SPC-130 EM) by focusing through a 75-μm pinhole and fluorescence filter (FELH0650, Thorlabs) to block scattered excitation light. Each sample was measured for 60 s.

Computational Methods. Density functional theory (DFT) calculations were employed in the gas phase to optimize the backbone geometry and calculate the frontier molecular orbitals (FMOs) on three units of **P2TI** and **P2TITT** using Gaussian 16/C01.[17] The geometry optimization calculations were carried out using the B3LYP hybrid functional and 6-31g(d) basis set, after reducing the alkyl side chain lengths to single methyl units, as their contribution to the electron density of the polymer is negligible.[18] For the density of states (total/partial density-of-state (TDOS/PDOS)) calculations, the CAM-B3LYP functional was used instead. Geometry optimization and frequency calculations were performed until a stationary point was found for both calculations. The excited-state properties and the UV−vis absorption spectra of the oligomers were analyzed using time-

https://doi.org/10.1021/acs.jpcc.4c04825
J. Phys. Chem. C 2024, 128, 16904−16914

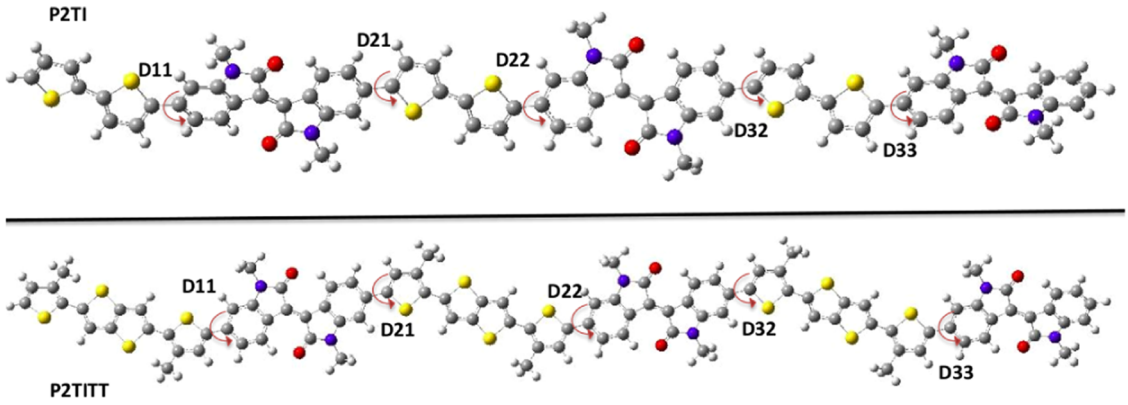

Figure 1. Optimized geometries and dihedral angles D_{ij} between the donor and acceptor units for 3-unit oligomers of the two polymers, where i and j represent the donor and acceptor units, respectively; red (O), blue (N), yellow (S) and gray (C).

dependent density functional theory (TD-DFT) with the CAM-B3LYP functional and 6-31g(d) basis set.

RESULTS AND DISCUSSION

Backbone Conformation and Electrochemistry. The degree of conjugation and planarity of copolymers are key factors that determine their potential applications as well as their charge-transfer and self-aggregation characteristics.[19,20] The planarity of the copolymers **P2TI** and **P2TITT** was evaluated using the DFT-optimized backbone geometries, which were obtained using the B3LYP functional and 6-31g(d) basis set as displayed in Figure 1.

To quantitatively characterize the planarity of the polymers, two metrics were employed: the molecular planarity parameter (MPP) and the span of deviation from the plane (SDP).[21] The MPP reflects the overall deviation of the molecular structure from a fitting plane, while the SDP represents the deviation span of the structure relative to the fitting plane. Generally, a more planar molecular structure is expected to exhibit lower values for both the MPP and the SDP.[22−24] The introduction of a thieno[3,2-*b*]thiophene (**TT**) spacer between the two thiophene rings of the donor unit was found to significantly affect the MPP and SDP values resulting in MPP and SDP values, respectively, of 0.91 and 5.25 Å in **P2TI**, and 0.73 and 4.07 Å in **P2TITT**. Notably, the incorporation of a **TT** spacer between the thiophene rings of the donor unit was found to planarize the copolymer by minimizing intramolecular steric hindrance between the acceptor and the donor units. To understand the origin of the backbone twist in **P2TI** the dihedral angles D_{ij} (where i and j represent the labels of the donor and acceptor units, respectively, denoted in Figure 1), were measured from the optimized geometries and summarized in Table 1. The results indicate that the dihedral angles between the donor and acceptor units of the copolymers were not significantly affected by the spacer. However, the introduction of the TT spacer notably enhanced the overall planarity, as evident from the side views of the optimized trimers of each polymer shown in Figure S1.

Table 1. Dihedral Angles (°) between the Thiophene and Isoindigo Units in the Trimer Units as Denoted in Figure 1

dihedral angle (°)	P2TI	P2TITT
D11	158.73	158.94
D21	158.82	158.50
D22	159.04	159.31
D32	159.18	158.38
D33	158.95	158.78

In addition to the backbone conformation, π-spacers are also known to affect the electrical and optical properties of polymers. Thus, the frontier molecular orbitals (FMOs) of **P2TI** and **P2TITT** were computed using the B3LYP functional and 6-31g(d) basis set, and the results are shown in Figure S2 along with the experimentally obtained values.[25,26] The experimental highest occupied molecular orbital (HOMO) and lowest unoccupied molecular orbital (LUMO) energy levels were investigated using squarewave voltammetry (SWV) with their values calculated from the onsets of their oxidation and reduction potentials, respectively, using eq 1 as reported by Bekri et al. and Desalegn et al.[25,26]

$$E_{\mathrm{HOMO/LUMO}} = -(E_{\mathrm{red}}^{\mathrm{ox}} \pm 4.4)\ \mathrm{eV} \quad (1)$$

In addition to determining the energy levels of FMOs, the spatial distribution of the electron density in these FMOs plays a major role in the electron-transfer processes in donor−acceptor copolymer systems. This is because intramolecular charge transfer occurs through the transfer of electron density from the donor to the acceptor moieties.[27] The incorporation of **TT** between the two thiophene rings in the donor unit was found to raise the HOMO energy level of the copolymer compared to **P2TI**, indicating an enhanced electron-donating capability, corroborating previous studies.[28,29] In contrast, the introduction of the electron-rich **TT** bridge had only a slight influence on the LUMO energy level, confirming that the LUMO level is primarily determined by the electron-deficient acceptor unit.[30,31] Similar findings were reported by Tao et al.[30] who observed that the DFT-calculated LUMO levels of isoindigo-based copolymers were quite comparable. Notably, the DFT-calculated FMO energies closely followed the trend observed in the experimental data, as shown in Figure S2.

Furthermore, the electron cloud distributions in the FMO surfaces of **P2TI** and **P2TITT**, depicted in Figures S3 and S4, reveals that the HOMOs of the two copolymers are delocalized along the π-conjugated backbone. In contrast, their LUMOs are primarily concentrated on the isoindigo-based acceptor unit, indicating efficient intramolecular charge transfer in these D−A copolymers. To further evaluate the contributions of the donor and acceptor units to the electron cloud distribution in the FMOs, we calculated the partial and total density of states (PDOS and TDOS, red in Figure 2) for each copolymer using

https://doi.org/10.1021/acs.jpcc.4c04825
J. Phys. Chem. C 2024, 128, 16904−16914

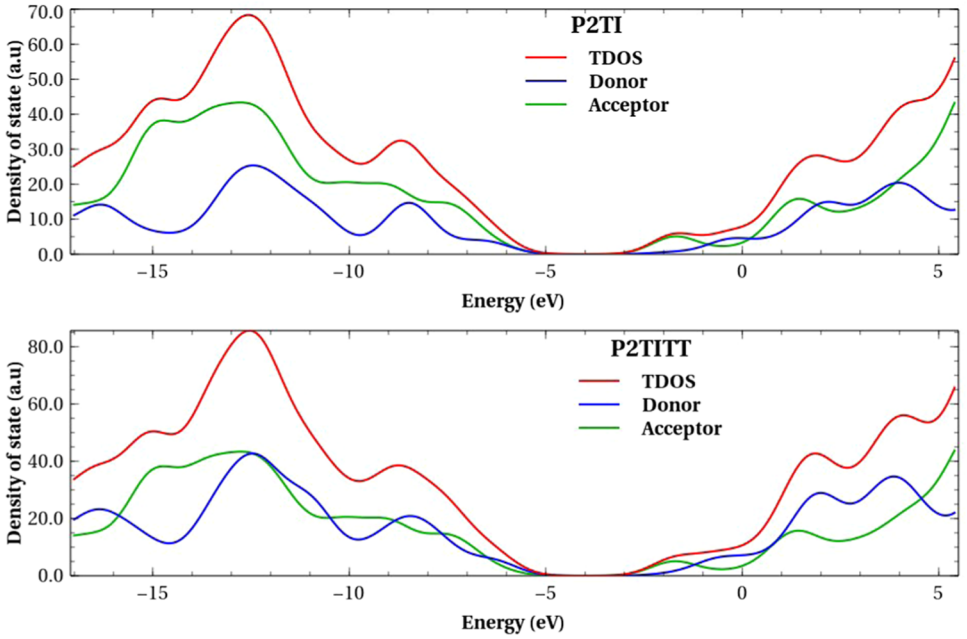

Figure 2. Total density of states in trimeric units of **P2TI** and **P2TITT** along with partial density of states of the donor and acceptor moieties, calculated using CAM-B3LYP/6-31g(d).

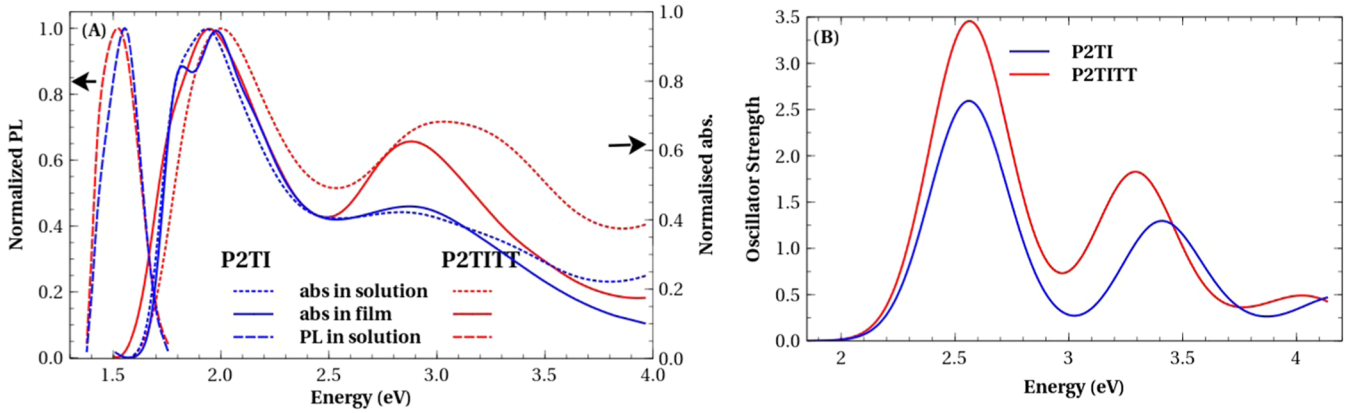

Figure 3. (A) Experimental absorption spectra in solution (dotted lines) and thin films (solid lines), and PL spectra (dashed lines) in solution of **P2TI** (blue) and **P2TITT** (red) and (**B**) TD/DFT-calculated absorption of the copolymers in 3 units.

the CAM-B3LYP/6-31g(d) functional by fragmenting the polymer into donor (blue) and acceptor (green) components, as shown in Figure 2. The density distribution of the valence band (HOMO) and the conduction band (LUMO) are represented by the negative and positive *x*-axes, respectively. Both in **P2TI** and **P2TITT**, the TDOS occupies more space on the valence band than the conduction band, which supports the donating property of the copolymers. Comparing the TDOS of the two copolymers further reveals **P2TITT** has a stronger donating capacity, as evidenced by a higher TDOS amplitude in the valence band. This finding is analogous to previous studies on acceptors in which the density of state rather occupies more space on the conduction band.[32,33] The analysis reveals that the contribution of the donor unit to the electron density in the HOMO level increased from 47.8% in **P2TI** to 58.4% in **P2TITT** confirming a more localized HOMO in the **TT**-spaced copolymer **P2TITT**. The localization of the HOMO level in **P2TITT** is expected to enhance the intramolecular charge transfer in this material. In contrast, the contribution of the acceptor unit to the LUMO level decreased from 87.3% to 77.5% due to the inclusion of the **TT** spacer.

The energy levels of the copolymers are a direct result of the electron distribution at each atomic site within the polymer structure. Therefore, calculating the electrostatic potential (ESP) is an important tool to quantify the differences between the two polymers.[34,35] The ESP surface for three repeat units of **P2TI** and **P2TITT**, calculated at the B3LYP/6-31g(d) level of theory, are shown in Figure S5. Interestingly, the ESP values of the donor units were found to be less negative in the **P2TI** copolymer compared to **P2TITT**. This indicates a stronger electron-donating affinity of the **P2TITT** copolymer as a result of incorporating the **TT** spacer units. Consequently, the HOMO level of the **P2TITT** copolymer was found to shift upward as observed in Figure S2.[28,36] Intriguingly, the isoindigo units in the two copolymers displayed different ESP values, suggesting that the intramolecular charge-transfer process has modulated the electron distribution along the polymer backbone. This agrees with the electron cloud distribution in the FMO surfaces shown in Figures S3 and S4.

https://doi.org/10.1021/acs.jpcc.4c04825
J. Phys. Chem. C 2024, 128, 16904−16914

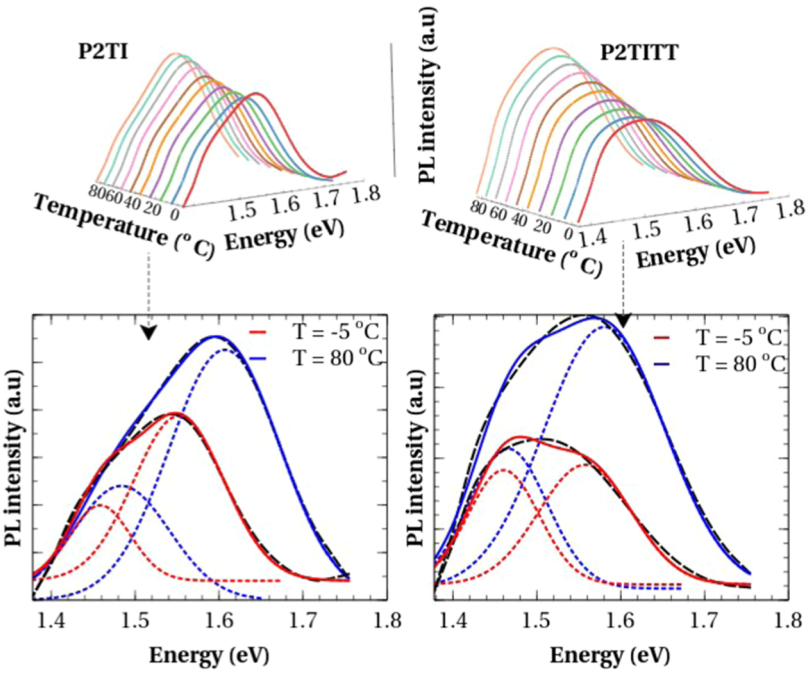

Figure 4. Temperature-dependent PL spectra over a temperature range of −5 to 85 °C (top panels) and two-peak Gaussian fit (bottom panels) at −5 (red) and 80 °C (blue) of **P2TI** (left) and **P2TITT** (right). The dashed, solid, and dotted lines represent the measured data, the cumulative fit, and the two distinct bands, respectively.

In summary, the analysis indicates that the **TT** bridges play an important role in imparting increased planarity to the bithiophene-isoindigo-based copolymer **P2TITT**. Moreover, the incorporation of the **TT** spacer enhances the electron-donating strength of the donor units, which increased the energy of the HOMO level compared to the **P2TI** copolymer. This is also supported by a higher density of states in **P2TITT** compared to **P2TI** in the valence band. The more planar molecular geometry facilitated by the **TT**-bridge is anticipated to improve the charge mobility in the **P2TITT** copolymer.

Absorption. To further investigate the optoelectronic properties, TD-DFT calculations were performed on trimer units of **P2TI** and **P2TITT** using the CAM-B3LYP/6-31g(d) functional in the gaseous state. The results are plotted in Figure 3B. The **TT**-spaced copolymer **P2TITT** was found to exhibit a higher oscillator strength than **P2TI**. The $S_0 \rightarrow S_1$ transition occurred at 2.56 eV for **P2TI** and 2.55 eV for **P2TITT** indicating that the **TT** spacer has a negligible effect on the optical band gap. In contrast, there are clear differences in the electrochemical band gap calculated from $E_{gap}^{EC} = E_{LUMO} - E_{HOMO}$, where in the case of **P2TI**, the transition to the first excited state consists of H(OMO) → L(UMO) and H − 1 → L+1 transitions with contributions of 52.5 and 18.2%, respectively, and in **P2TITT**, the H → L, H − 1 → L+1, and H − 3 → L+1 transitions comprise the first excited state with respective contributions of 40.7, 14.7, and 10.8%. As depicted in Figures S3 and S4, while the HOMO orbitals are delocalized over the backbone and HOMO−1 is slightly shifted toward the donor units, the LUMO orbital is highly localized on the isoindigo acceptor unit. This confirms that the first excited state in both polymers is predominantly an intramolecular charge-transfer (ICT) state.

The absorption spectra of **P2TI** and **P2TITT** were measured in both solution and thin film, while the PL spectra of the two copolymers were obtained in solution, as shown in Figure 3A. Both copolymers display the common two-band absorption features that originate from ICT and local $\pi-\pi^*$ transitions. The ICT double-band of the thin film is particularly evident for **P2TI** and indicates the formation of aggregates in the thin films. In solution, the absorption spectrum of **P2TI** is red-shifted compared to **P2TITT**. Conversely, **P2TI**'s thin film absorption spectrum is blue-shifted relative to that of **P2TITT**. Because thin films usually give rise to strong interchain $\pi-\pi$ interaction,[15] the opposite trend between the solution- and thin-film-based absorption spectra can be attributed to the following potential reasons: (i) **P2TI** in solution already exhibits strong $\pi-\pi$ stacking, which is negligibly enhanced in the thin film, leading to a negligible additional red shift, whereas in **P2TITT**, the thin film produces stronger aggregation, resulting in a more pronounced red shift. (ii) The trend observed in thin films agrees with the DFT-calculated results, confirming that the **TT** spacer narrows the band gap in **P2TITT**. The opposite trend in solution could be related to solvation effects.

The PL spectra of the two copolymers in solution (Figure 3A) reveal broader and more red-shifted emission for **P2TITT** compared to **P2TI**. This may arise from additional vibrational modes introduced by the **TT** spacer.

Furthermore, the Stokes shifts were calculated to be 0.38 eV for **P2TI** and 0.47 eV for **P2TITT**. The larger Stokes shift of **P2TITT** suggests that it undergoes more intraband relaxation prior to emission compared to **P2TI**. According to Kasha's model, emission occurs from the band minimum, where the band necessarily has positive curvature.[37,38] To distinguish between J- and H-type aggregation, the free-exciton band curvature at the band minimum can be evaluated from the second derivative of the energy using eq 2,[39]

$$\omega_c \equiv \frac{1}{2}\frac{d^2E_k}{dk^2}\bigg|_{k=k_{min}} \quad (2)$$

https://doi.org/10.1021/acs.jpcc.4c04825
J. Phys. Chem. C 2024, 128, 16904−16914

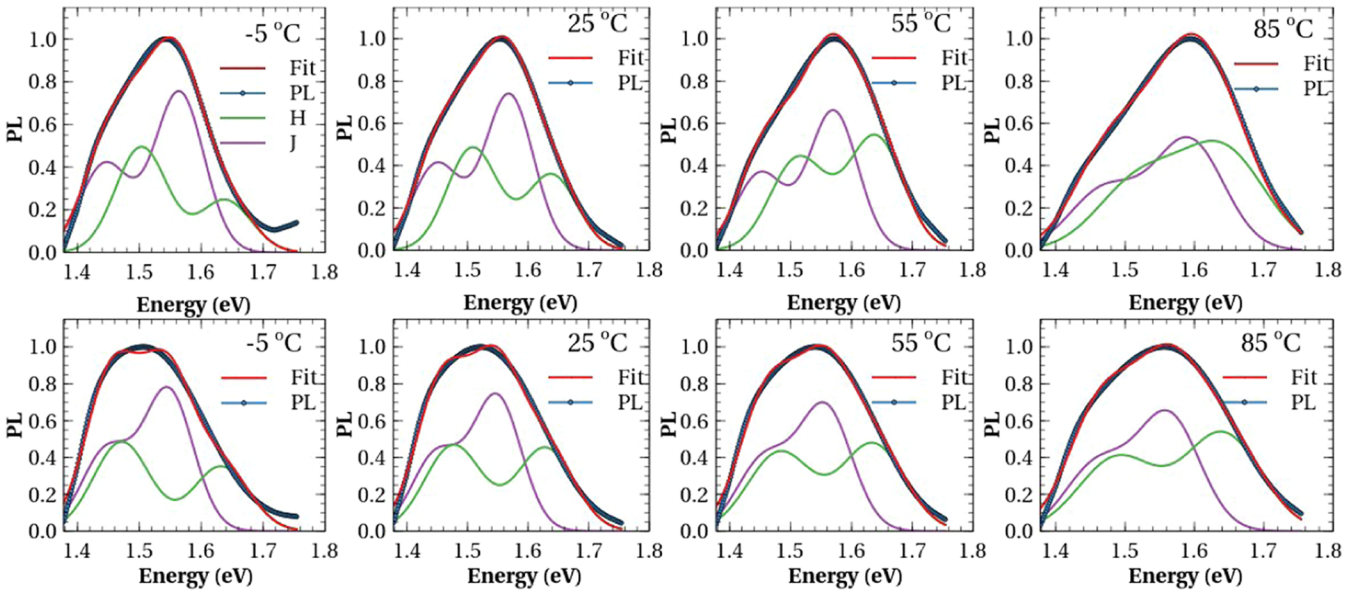

Figure 5. Franck−Condon curve fits at selected temperatures of **P2TI** (top) and **P2TITT** (bottom).

where ω_c is the band curvature, k is the wavenumber, and E_k the energy at the kth exciton.

In J-aggregates, since the $k = 0$ exciton defines the band minimum, the free-exciton curvature is positive at the band bottom. Hence, emission occurs directly from the $k = 0$ exciton with negligible Stokes shift. In contrast, for H-aggregates, the $k = 0$ state resides at the top of the band giving a negative curvature. Therefore, in H-aggregates, emission will be possible only in the presence of symmetry-breaking disorder or vibronic coupling due to intraband relaxation that populates excitons from the $k = 0$ to the $k = \pi$ band. In this regard, the chromophores in both **P2TI** and **P2TITT** might assemble preferably in an H-type aggregate form, with the symmetry-breaking disorder potentially being greater in **P2TI**. Alternatively, the shift in the potential wells between the ground state and excited states could be more substantial in **P2TITT** than **P2TI** leading to the observed larger Stokes shift for **P2TITT**.

Temperature-Dependent Photoluminescence. The aggregation type of polymers can be determined by analyzing the evolution of the 0−0 and 0−1 emission peaks (I_{00} and (I_{01}), respectively) as a function of temperature. To this end, the temperature-dependent PL spectra of the two copolymers were recorded in solution over the temperature range of −5 to 85 °C in steps of 10 °C as depicted in Figure 4. To assess the effect of temperature on the vibronic peak energy and intensity, a two-peak Gaussian fit was carried out at the end temperatures, $T = -5$ and 80 °C, as shown in the bottom panels of Figure 4. As the temperature increased from −5 to 85 °C, the main emission peak (I_{00}) of both **P2TI** and **P2TITT** exhibited a blue-shift by 51.54 and 49.15 meV, respectively, accompanied by spectral broadening and increased intensity. The blue-shift of the emission peak can be attributed to a decrease in the effective conjugation length due to thermally induced dissociation of interchain couplings, while the broadening and intensity increase are likely due to the liberation of new emissive states facilitated by the elevated temperature.[40−42]

A cursory examination of the PL spectra reveals that the I_{00} peak intensity dominates over the I_{01} peak intensity, characteristic of J-aggregate formation. However, the observation that the I_{00} intensity increases with rising temperature also suggests H-aggregate characteristics, because the 0−0 transition is optically forbidden in an ideal H-aggregate, but as temperature increases, the amount of disorder increases and the transition becomes more likely. To gain deeper insight into the aggregation behavior, a Franck−Condon analysis was employed to curve-fit the temperature-dependent PL spectra. This analysis utilized two Franck−Condon progressions to account for the potential coexistence of both J- and H-type aggregates in the copolymers, as given by eqs 3 and 4.[43−45]

$$I_J(\hbar\omega) \propto (\hbar\omega)^3 n^3 \exp(-S)\left(\sum_{m=0} \frac{S^m}{m!}\Gamma(\hbar\omega - E_0 + mE_p)\right) \tag{3}$$

$$I_H(\hbar\omega) \propto (\hbar\omega)^3 n^3 \exp(-S)\left(\alpha\Gamma(\hbar\omega - E_0) + \sum_{m=1} \frac{S^m}{m!}\Gamma(\hbar\omega - E_0 + mE_p)\right) \tag{4}$$

where n is the real part of the refractive index at photon energy $\hbar\omega$, m denotes the vibrational level, S is the HR factor, which gives a measure of the coupling between the electronic transition and a phonon mode, E_0 is the 0−0 transition energy, E_p is the phonon energy, and Γ is a Gaussian line shape with constant width. The parameter α is the exciton coherence number, which appears only in the modified Franck−Condon model and denotes the competition between intra- and interchain exciton coupling. It is a function of disorder and dictates the intensity of I_{00}, which is absent for a perfectly ordered H-aggregate at 0 K. The common phonon mode available in almost all conjugated polymers (ω = 1400 cm^{-1}) was used in the fitting.

As shown in Figure 5, the PL spectra of **P2TI** and **P2TITT** were successfully fitted with H-type and J-type Franck−Condon progressions at some representative temperatures.

https://doi.org/10.1021/acs.jpcc.4c04825
J. Phys. Chem. C 2024, 128, 16904−16914

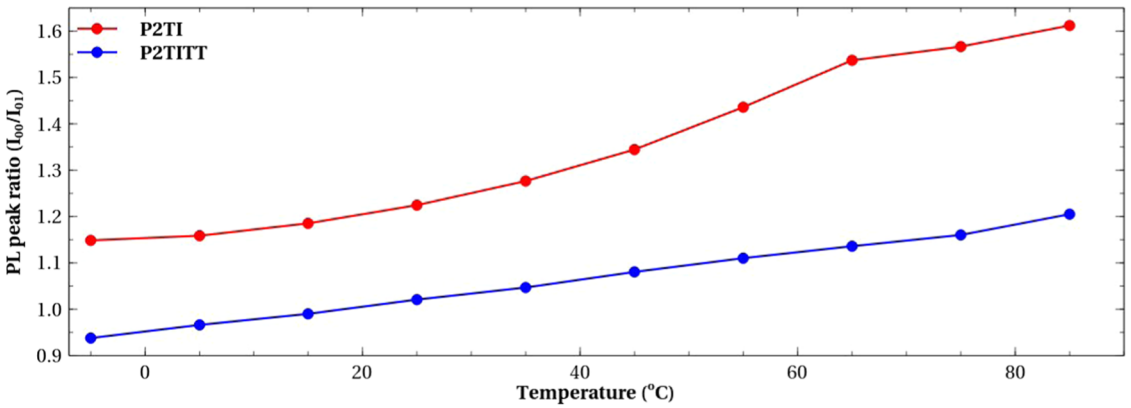

Figure 6. Temperature-dependent PL peak ratios calculated after Franck−Condon curve fits.

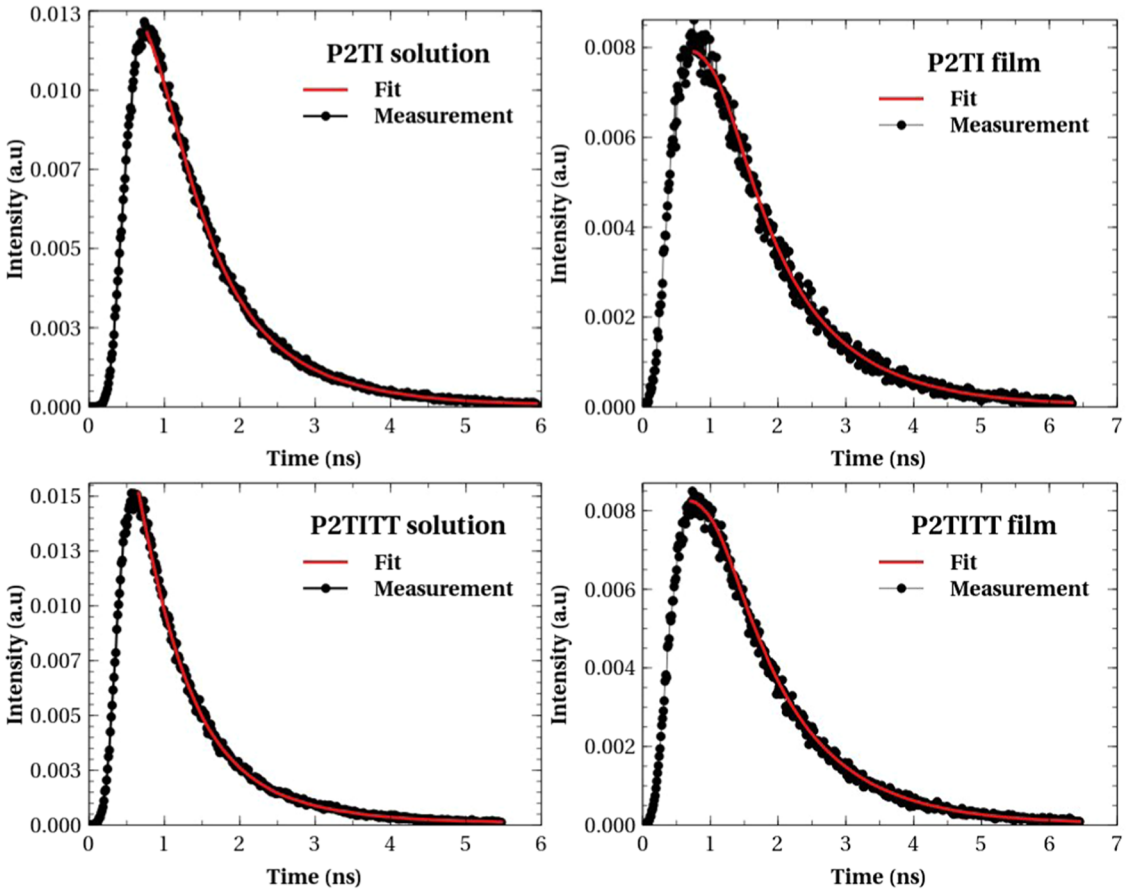

Figure 7. Emission decay curves fitted with two exponential functions.

This suggests that both H- and J-type aggregates are present in the polymers. Upon increasing temperature, an enhancement in the 0−0 peak emission intensity occurred, particularly for the H-type spectral component. This is likely due to thermal disorder-induced relaxation of the selection rules, which makes the 0−0 transition more allowed. In other words, an enhanced I_{00} intensity can be attributed to a decrease in interchain interaction.[46] The PL peak ratio (I_{00}/I_{01}) calculated from the curve fits is plotted in Figure 6. This ratio is higher for **P2TITT** than for **P2TI**, indicating higher temperatures are required to break the symmetry in **P2TITT**, consistent with the greater Stokes shift of **P2TITT** in Figure 3A. A similar study on anthracene-containing statistical poly(phenylene ethynylene)-*alt*-(phenylenevinylene) (AnE-PVstat) copolymers in solution revealed an increase in the I_{00}/I_{01} ratio which the authors attributed to a reduction in the interchain interaction potentially leading to a breakdown of H-aggregates.[46]

Figure 6 also indicates a more gradual increase in the PL peak ratio with temperature for **P2TITT** than for **P2TI**, from which it can be inferred that the **TT**-spaced copolymer **P2TITT** exhibits stronger interchain interactions than **P2TI**. This could be due to the more planar geometry of **P2TITT**, which would suppress molecular torsion upon increasing temperature.[46]

https://doi.org/10.1021/acs.jpcc.4c04825
J. Phys. Chem. C 2024, 128, 16904−16914

As pointed out in the work of Kanemoto et al. on 16-mer oligothiophene (16 T),[42] the full width at half-maximum (fwhm) of the emission spectra can be used to assess conformational changes induced by temperature. In this regard, the fwhm values were extracted from the Franck−Condon fits of the PL spectra. The results show that **P2TITT** exhibits higher fwhm values than **P2TI**, supporting the broader PL spectra of **P2TITT** due to the presence of additional phonon modes. Moreover, the fwhm increases with rising temperature for both **P2TI** and **P2TITT**, as higher temperatures lead to increased conformational disorder. Specifically, the fwhm of **P2TI** increased from 40.80 to 45.90 meV (a 12.50% increase), while for **P2TITT** it increased from 42.60 to 46.10 meV (an 8.22% increase), over the measured temperature range. These results suggest that the temperature-induced conformational changes are more pronounced in **P2TI** than in **P2TITT**.

Another parameter used to compare the exciton interchain coupling in the copolymers is α, which dictates the intensity of the I_{00} peak as described in eq 4. The value of α can range from 0 to 1, with 0 indicating complete dominance of interchain interaction and perfect H-aggregate formation, while 1 would suggest the dominance of intrachain interaction. Over the measured temperature range, the value of α increased from 0.46 to 0.98 for **P2TI** and from 0.35 to 0.87 for **P2TITT**. Smaller values of α for **P2TITT** than **P2TI** at any temperature further supports the notion that interchain exciton coupling is stronger in **P2TITT** than in **P2TI**.[44]

Emission Lifetimes. Time-resolved PL measurements were performed on diluted solutions and films of **P2TI** and **P2TITT**. The emission decay profiles were best fitted using biexponential functions convolved with a simulated instrument response function (IRF) using the software described in ref 47. The fitted function is of the form

$$\mathrm{IRF} \otimes (A_1 e^{-t/\tau_1} + A_2 e^{-t/\tau_2}) \quad (5)$$

where A and τ are fitting parameters representing the fraction of molecules decaying and the corresponding PL lifetime, respectively.

The experimental PL decay curves along with their corresponding biexponential fits are presented in Figure 7. Small values of χ^2 close to unity and lack of structure in the residuals were used to confirm the goodness of the fits. The extracted lifetime values are also summarized in Table 2. Since, we are considering donor copolymers, not blends, factors such as bimolecular recombination and carrier traps may not have significant effects because we do not expect free charge carriers and carrier traps, especially in solution. Hence, the presence of two distinct lifetimes in the decay profile may suggest the coexistence of two different types of aggregation species, namely H- and J-aggregates, within the polymers. However, as mentioned in the experimental section, the polymer solutions were prepared at a relatively low concentration of approximately 0.02 mg/mL, which is unlikely to promote significant aggregation. Therefore, the two observed lifetime components in the solution-phase measurement can be more appropriately assigned to isolated (non-aggregated) polymer chains for fast decaying and H-aggregated polymer chains for long-lived components.

Table 2. Lifetimes and Corresponding Amplitudes of the Copolymers

		τ_1 (ns)	A_1 (%)	τ_2 (ns)	A_2 (%)	average τ (ns)
P2TI	solution	0.34	66	1.01	34	0.57
	film	0.30	50	1.10	50	0.70
P2TITT	solution	0.46	80	1.01	20	0.57
	film	0.26	47	1.09	53	0.70

A closer examination of the relative amplitudes of the two lifetime components revealed that the faster decays tend to dominate over the longer lifetimes in the solution state as evidenced by the higher pre-exponential factors ($A_1 > A_2$) associated with the shorter lifetime species. Attributing the longer lifetimes to H-aggregated species[11] and the shorter lifetimes to isolated chain segments, the increase in the amplitude of the longer lifetime component in the thin films compared to solution suggests that the proportion of aggregated species increases in the solid state.

Similar assignments of longer lifetimes to aggregated species and shorter lifetimes to non-aggregated chain segments have been reported in the literature for other polymer systems.[48−50] For example, in poly(*p*-pyridyl vinylene) (PPyV), the solution-phase PL decay was found to be nearly monoexponential while the film emission consisted of both very fast and long-lived species.[48] Likewise, in PPE−PPV copolymers, the emission lifetimes in solution were well-described by single-exponential decays assigned to H-aggregated species, whereas the lifetimes in the film were better fitted using a bi-exponential function, with the longer lifetime component attributed to H-aggregate and the shorter lifetime to J-aggregated chain segments.[49,50]

The need to employ a bi-exponential function to fit the PL decay profiles of the **P2TI** and **P2TITT** copolymers further supports the presence of two distinct emissive species, likely corresponding to H-aggregated and isolated chain segments in the solution state or H-aggregated and J-aggregated (isolated chain) segments in the thin film as the photophysical properties of single conjugated polymer chains and J-aggregates are similar.[51] The notion of two distinct emissive species is consistent with the Franck−Condon analysis of the temperature-dependent PL spectra.

CONCLUSIONS

In this work, we have studied the effect of backbone conformation on aggregation-induced photophysics of two isoindigo-based bithiophene-isoindigo copolymers with (**P2TITT**) and without (**P2TI**) **TT** spacer. The introduction of a **TT** spacer in **P2TITT** improved the planarity of the copolymer backbone and shifted the HOMO energy level upward due to the stronger electron-donating nature of the **TT** moiety. These structural and electronic changes also affected the extent of HOMO−LUMO delocalization in the two copolymers. To probe the aggregation behavior of these materials, temperature-dependent photoluminescence measurements were conducted. The temperature-dependent evolution of the key parameters such as the intensity ratio of the first two vibronic peaks, the peak positions, and spectral broadening provided insights into the temperature-induced changes in the effective conjugation length and the activation of more emissive conformational species due to the dissociation of interchain couplings. Interestingly, a comparison of the temperature-dependent PL peak ratios between the two copolymers revealed stronger interchain interaction in the **TT**-containing **P2TITT**. Furthermore, the PL spectra were

https://doi.org/10.1021/acs.jpcc.4c04825
J. Phys. Chem. C 2024, 128, 16904−16914

best fitted using two Franck−Condon progressions suggesting the coexistence of two distinct aggregation types, which was further supported by the observation of two emission lifetime components in the time-resolved PL measurements. The longer lifetime component was attributed to H-aggregate species, while the shorter lifetime was assigned to J-aggregate (isolated) chain segments. The relative contributions of these lifetime components, as reflected in the pre-exponential factors, indicated that the proportion of aggregated species increases in the thin films compared to the dilute solutions. These findings provide valuable insights into the role of the backbone conformation and interchain interaction in modulating the aggregation-induced photophysical properties of conjugated polymers, which is crucial for their optimization in optoelectronic applications.

■ ASSOCIATED CONTENT

Supporting Information

The Supporting Information is available free of charge at https://pubs.acs.org/doi/10.1021/acs.jpcc.4c04825.

Side view of the optimized geometry, DFT-calculated and experimental HOMO−LUMO levels, electron cloud distribution and electrostatic potential surface for trimeric units of the two polymers (PDF)

■ AUTHOR INFORMATION

Corresponding Author

Newayemedhin A. Tegegne − *Department of Physics, Addis Ababa University, 1176 Addis Ababa, Ethiopia;* orcid.org/0000-0002-5822-9145; Email: newaye.medhin@aau.edu.et

Authors

Eninges Asmare − *Department of Physics, Addis Ababa University, 1176 Addis Ababa, Ethiopia; Department of Physics, Wollo University, Dessie 1145, Ethiopia;* orcid.org/0000-0001-6126-3128

Nika Bekri − *Department of Mathematics, Physics and Statistics, Sustainable Energy Center of Excellence, and Nano Technology Center of Excellence, Addis Ababa Science and Technology University, 16417 Addis Ababa, Ethiopia*

Leonato Tambua Nchinda − *Department of Physics, University of Pretoria, Pretoria 0083, South Africa*

Fekadu G. Hone − *Department of Physics, Addis Ababa University, 1176 Addis Ababa, Ethiopia*

Wendimagegn Mammo − *Department of Chemistry, Addis Ababa University, 33658 Addis Ababa, Ethiopia*

Tjaart P. J. Krüger − *Department of Physics, University of Pretoria, Pretoria 0083, South Africa; National Institute for Theoretical and Computational Sciences, (NITheCS), South Africa;* orcid.org/0000-0002-0801-6512

Complete contact information is available at: https://pubs.acs.org/10.1021/acs.jpcc.4c04825

Author Contributions

E.A. wrote the first draft in addition to conducting the computational and experimental research for the work. W.M. guided the synthesis of the polymers. N.A.T. and T.P.J.K. conceptualized the project and oversaw its completion. All authors contributed to the data analysis, discussion, and editing of the final manuscript.

Notes

The authors declare no competing financial interest.

■ ACKNOWLEDGMENTS

This work was based on support from the National Institute of Technology and Computational Sciences (NITheCS). Calculations were performed on the South African Department of Science and Innovation (DSI)'s Centre for High Performance Computing in Cape Town. We also acknowledge the International Science Program (ISP), Uppsala University, Sweden, for providing the laboratory facilities for the polymer physics laboratory in the Department of Physics at Addis Ababa University. W.M. would also like to acknowledge ISP for financial support.

■ REFERENCES

(1) Khasbaatar, A.; Xu, Z.; Lee, J.-H.; Campillo-Alvarado, G.; Hwang, C.; Onusaitis, B. N.; Diao, Y. From Solution to Thin Film: Molecular Assembly of π-Conjugated Systems and Impact on (Opto) electronic Properties. *Chem. Rev.* **2023**, *123*, 8395−8487.

(2) Luo, S.; Li, C.; Zhang, J.; Zou, X.; Zhao, H.; Ding, K.; Huang, H.; Song, J.; Yi, J.; Yu, H.; et al. Auxiliary sequential deposition enables 19%-efficiency organic solar cells processed from halogen-free solvents. *Nat. Commun.* **2023**, *14*, No. 6964.

(3) Liu, K.; Jiang, Y.; Ran, G.; Liu, F.; Zhang, W.; Zhu, X. 19.7% efficiency binary organic solar cells achieved by selective core fluorination of nonfullerene electron acceptors. *Joule* **2024**, *8*, 835−851.

(4) Yang, J.; Wang, X.; Yu, X.; Liu, J.; Zhang, Z.; Zhong, J.; Yu, J. Improved Short-Circuit Current and Fill Factor in PM6: Y6 Organic Solar Cells through D18-Cl Doping. *Nanomaterials* **2023**, *13*, 2899.

(5) Xie, B.; Zhang, K.; Hu, Z.; Fang, H.; Lin, B.; Yin, Q.; He, B.; Dong, S.; Ying, L.; Ma, W.; et al. Polymer pre-aggregation enables optimal morphology and high performance in all-polymer solar cells. *Solar RRL* **2020**, *4*, No. 1900385.

(6) Guo, C.; Fu, Y.; Li, D.; Wang, L.; Zhou, B.; Chen, C.; Zhou, J.; Sun, Y.; Gan, Z.; Liu, D.; et al. A Polycrystalline Polymer Donor as Pre-Aggregate toward Ordered Molecular Aggregation for 19.3% Efficiency Binary Organic Solar Cells. *Adv. Mater.* **2023**, *35*, No. 2304921.

(7) Song, C.-p.; Qu, Y.; Liu, J.-g.; Han, Y.-c. Phase-separation mechanism and morphological control in all-polymer solar cells. *Acta Polym. Sin.* **2018**, 145−163.

(8) Park, K. S.; Kwok, J. J.; Dilmurat, R.; Qu, G.; Kafle, P.; Luo, X.; Jung, S.-H.; Olivier, Y.; Lee, J.-K.; Mei, J.; et al. Tuning conformation, assembly, and charge transport properties of conjugated polymers by printing flow. *Sci. Adv.* **2019**, *5*, No. eaaw7757.

(9) Ma, R.; Jiang, X.; Fu, J.; Zhu, T.; Yan, C.; Wu, K.; Müller-Buschbaum, P.; Li, G. Revealing the underlying solvent effect on film morphology in high-efficiency organic solar cells through combined ex situ and in situ observations. *Energy Environ. Sci.* **2023**, *16*, 2316−2326.

(10) Zhao, Q.; Lai, H.; Chen, H.; Li, H.; He, F. H-and J-aggregation inspiring efficient solar conversion. *J. Mater. Chem. A* **2021**, *9*, 1119−1126.

(11) Zhao, Q.; Liu, J.; Wang, H.; Li, M.; Zhou, K.; Yang, H.; Han, Y. Balancing the H-and J-aggregation in DTS (PTTh 2) 2/PC 70 BM to yield a high photovoltaic efficiency. *J. Mater. Chem. C* **2015**, *3*, 8183−8192.

(12) Pan, S.; Zhu, M.; He, L.; Zhang, H.; Qiu, F.; Lin, Z.; Peng, J. Transformation from nanofibers to nanoribbons in poly (3-Hexylthiophene) solution by adding alkylthiols. *Macromol. Rapid Commun.* **2018**, *39*, No. 1800048.

(13) Chang, M.; Lee, J.; Kleinhenz, N.; Fu, B.; Reichmanis, E. Photoinduced anisotropic supramolecular assembly and enhanced charge transport of poly (3-hexylthiophene) thin films. *Adv. Funct. Mater.* **2014**, *24*, 4457−4465.

(14) Ziffer, M. E.; Jo, S. B.; Liu, Y.; Zhong, H.; Mohammed, J. C.; Harrison, J. S.; Jen, A. K.-Y.; Ginger, D. S. Tuning H-and J-aggregate behavior in π-conjugated polymers via noncovalent interactions. *J. Phys. Chem. C* **2018**, *122*, 18860−18869.
(15) Tegegne, N. A.; Abdissa, Z.; Mammo, W.; Uchiyama, T.; Okada-Shudo, Y.; Galeotti, F.; Porzio, W.; Andersson, M. R.; Schlettwein, D.; Vohra, V.; Schwoerer, H. Effect of alkyl side chain length on intra-and intermolecular interactions of terthiophene-isoindigo copolymers. *J. Phys. Chem. C* **2020**, *124*, 9644−9655.
(16) Kyeyune, F.; Botha, J. L.; Van Heerden, B.; Malỳ, P.; Van Grondelle, R.; Diale, M.; Krüger, T. P. Strong plasmonic fluorescence enhancement of individual plant light-harvesting complexes. *Nanoscale* **2019**, *11*, 15139−15146.
(17) Frisch, M. J.et al. *Gaussian˜16 Revision C.*; Gaussian Inc.: Wallingford CT, 2016.
(18) Ma, Z.; Geng, H.; Wang, D.; Shuai, Z. Influence of alkyl side-chain length on the carrier mobility in organic semiconductors: herringbone vs. π-π stacking. *J. Mater. Chem. C* **2016**, *4*, 4546−4555.
(19) Carlotti, B.; Cai, Z.; Kim, H.; Sharapov, V.; Madu, I. K.; Zhao, D.; Chen, W.; Zimmerman, P. M.; Yu, L.; Goodson, T., III Charge transfer and aggregation effects on the performance of planar vs twisted nonfullerene acceptor isomers for organic solar cells. *Chem. Mater.* **2018**, *30*, 4263−4276.
(20) Saeed, M. U.; Hadia, N.; Iqbal, J.; Hessien, M.; Shawky, A. M.; Ans, M.; Alatawi, N. S.; Khera, R. A. Impact of end-group modifications and planarity on BDP-based non-fullerene acceptors for high-performance organic solar cells by using DFT approach. *J. Mol. Model.* **2022**, *28*, 397.
(21) Lu, T. Simple, reliable, and universal metrics of molecular planarity. *J. Mol. Model.* **2021**, *27*, No. 263.
(22) Ishtiaq, M.; Waqas, M.; Zubair, H.; Mehmood, R. F.; Al-Zaqri, N.; Khera, R. A.; Ibrahim, M. A.; Iqbal, J. Theoretical designing of symmetrical non-fullerene acceptor molecules by end-capped modification for promising photovoltaic properties of organic solar cells. *J. Mol. Liq.* **2023**, *386*, No. 122473.
(23) Zhao, S.; Cao, J.; Liu, Q.; Zhang, X. Fine-tuning the π bridge of organic dye molecules with triarylamino as an electron donor by using electron-rich/deficient groups for more efficient dye-sensitized solar cells. *Mol. Phys.* **2022**, *120*, No. e2093286.
(24) Zaier, R.; Martel, A.; Antosiewicz, T. J. Effect of Benzothiadiazole-Based π-Spacers on Fine-Tuning of Optoelectronic Properties of Oligothiophene-Core Donor Materials for Efficient Organic Solar Cells: A DFT Study. *J. Phys. Chem. A* **2023**, *127*, 10555−10569.
(25) Bekri, N.; Asmare, E.; Abdissa, Z.; Mammo, W.; Tegegne, N. A. Photophysics and thermally-induced degradation of P2TI-DD, a polymer synthesized by direct arylation reaction. *J. Mater. Sci.: Mater. Electron.* **2022**, *33*, 16066−16076.
(26) Desalegn, B. S.; Bekri, N.; Hone, F. G.; Andoshe, D. M.; Mammo, W.; Abdissa, Z.; Bosman, G.; Tegegne, N. A. One-pot synthesis and thermal stability of thiophene-bridged thieno [3, 2-b] thiophene donor-based copolymers. *Mater. Today Commun.* **2021**, *29*, No. 102803.
(27) Chutia, T.; Ahmed, S.; Kalita, D. J. A Rational design of Dithieno-Benzo-Dithiophene based acceptors for organic solar cells. *Comput. Theor. Chem.* **2023**, *1228*, No. 114282.
(28) Tegegne, N. A.; Negash, A.; Yilma, D.; Gebremariam, K. G.; Genene, Z.; Mammo, W.; Goosen, N. J. Tailoring intra-molecular coupling in BDT-based copolymers to enhance their performance in fullerene-free organic solar cells. *Mater. Adv.* **2023**, *4*, 6694−6703.
(29) Zhou, N.; Guo, X.; Ortiz, R. P.; Harschneck, T.; Manley, E. F.; Lou, S. J.; Hartnett, P. E.; Yu, X.; Horwitz, N. E.; Burrezo, P. M.; et al. Marked consequences of systematic oligothiophene catenation in thieno [3, 4-c] pyrrole-4, 6-dione and bithiopheneimide photovoltaic copolymers. *J. Am. Chem. Soc.* **2015**, *137*, 12565−12579.
(30) Tao, Q.; Xia, Y.; Xu, X.; Hedstrom, S.; Backe, O.; James, D. I.; Persson, P.; Olsson, E.; Inganas, O.; Hou, L.; et al. D-A1-D-A2 copolymers with extended donor segments for efficient polymer solar cells. *Macromolecules* **2015**, *48*, 1009−1016.
(31) Blouin, N.; Michaud, A.; Gendron, D.; Wakim, S.; Blair, E.; Neagu-Plesu, R.; Belletete, M.; Durocher, G.; Tao, Y.; Leclerc, M. Toward a rational design of poly (2, 7-carbazole) derivatives for solar cells. *J. Am. Chem. Soc.* **2008**, *130*, 732−742.
(32) Bary, G.; Ghani, L.; Jamil, M. I.; Arslan, M.; Ahmed, W.; Ahmad, A.; Sajid, M.; Ahmad, R.; Huang, D. Designing small organic non-fullerene acceptor molecules with diflorobenzene or quinoline core and dithiophene donor moiety through density functional theory. *Sci. Rep.* **2021**, *11*, No. 19683.
(33) Khatua, R.; Das, B.; Mondal, A. Rational design of non-fullerene acceptors via side-chain and terminal group engineering: a computational study. *Phys. Chem. Chem. Phys.* **2023**, *25*, 7994−8004.
(34) Bora, S. R.; Kalita, D. J. End group modulation of A-D-A type small donor molecules for DTP based organic photovoltaic solar cells: a DFT approach. *RSC Adv.* **2023**, *13*, 26418−26429.
(35) Karaman, C. Z.; Göker, S.; Şahin, Ü.; Hacioglu, S. O.; Aslan, S. T.; Hacıefendioğlu, T.; Hizalan, G.; Yıldırım, E.; Çırpan, A.; Toppare, L. Effect of thiophene, 3-hexylthiophene, selenophene, and Thieno [3, 2-b] thiophene spacers on OPV device performance of novel 2, 1, 3-benzothiadiazole based alternating copolymers. *J. Electroanal. Chem.* **2021**, *895*, No. 115483.
(36) Tu, D.; Qiao, Y.; Ni, Y.; Guo, X.; Li, C. Structural engineering of anthracene diimide polymers for molecular ordering manipulation. *Macromolecules* **2022**, *55*, 4102−4110.
(37) McRae, E. G.; Kasha, M. Enhancement of phosphorescence ability upon aggregation of dye molecules. *J. Chem. Phys.* **1958**, *28*, 721−722.
(38) Kasha, M. Energy transfer mechanisms and the molecular exciton model for molecular aggregates. *Radiat. Res.* **1963**, *20*, 55−70.
(39) Hestand, N. J.; Spano, F. C. Expanded theory of H-and J-molecular aggregates: the effects of vibronic coupling and intermolecular charge transfer. *Chem. Rev.* **2018**, *118*, 7069−7163.
(40) Bencheikh, F.; Duché, D.; Ruiz, C. M.; Simon, J.-J.; Escoubas, L. Study of optical properties and molecular aggregation of conjugated low band gap copolymers: PTB7 and PTB7-Th. *J. Phys. Chem. C* **2015**, *119*, 24643−24648.
(41) Liu, L.; Han, T.; Wu, X.; Qiu, S.; Wang, B.; Hanif, M.; Xie, Z.; Ma, Y. Aggregation Behaviors of ladder-type poly (p-phenylene) in dilute solutions and spin-coated films. *J. Phys. Chem. C* **2015**, *119*, 11833−11838.
(42) Kanemoto, K.; Akai, I.; Sugisaki, M.; Hashimoto, H.; Karasawa, T.; Negishi, N.; Aso, Y. Temperature effects on quasi-isolated conjugated polymers as revealed by temperature-dependent optical spectra of 16-mer oligothiophene diluted in a sold matrix. *J. Chem. Phys.* **2009**, *130*, No. 234909.
(43) Yamagata, H.; Hestand, N. J.; Spano, F. C.; Köhler, A.; Scharsich, C.; Hoffmann, S. T.; Bässler, H. The red-phase of poly [2-methoxy-5-(2-ethylhexyloxy)-1, 4-phenylenevinylene](MEH-PPV): A disordered HJ-aggregate. *J. Chem. Phys.* **2013**, *139*, No. 114903.
(44) Clark, J.; Silva, C.; Friend, R. H.; Spano, F. C. Role of intermolecular coupling in the photophysics of disordered organic semiconductors: aggregate emission in regioregular polythiophene. *Phys. Rev. Lett.* **2007**, *98*, No. 206406.
(45) Asmare, E.; Hone, F. G.; Mammo, W.; Krüger, T. P.; Tegegne, N. A. Investigation into aggregation types in a benzodithiophene-isoindigo copolymer. *J. Chem. Phys.* **2023**, *159*, No. 034901.
(46) Saaidia, A.; Saidani, M.; Hleli, E.; Alam, S.; Ulbricht, C.; Romdhane, S.; Ben Fredj, A.; Kastner, C.; Egbe, D.; Schubert, U.; et al. Temperature-tuning of optical properties and molecular aggregation in AnE-PVstat copolymer solution. *J. Phys. Chem. C* **2018**, *122*, 3965−3969.
(47) Botha, J. L.; van Heerden, B.; Krüger, T. P. Advanced analysis of single-molecule spectroscopic data. *Biophys. Rep.* **2024**, *4*, No. 100173.
(48) Blatchford, J. W.; Gustafson, T.; Epstein, A.; Bout, D. V.; Kerimo, J.; Higgins, D.; Barbara, P.; Fu, D.-K.; Swager, T. M.; MacDiarmid, A. Spatially and temporally resolved emission from aggregates in conjugated polymers. *Phys. Rev. B* **1996**, *54*, No. R3683.

https://doi.org/10.1021/acs.jpcc.4c04825
J. Phys. Chem. C 2024, 128, 16904−16914

(49) Guesmi, M.; Fredj, A. B.; Romdhane, S.; Bouguerra, N.; Egbe, D.; Lang, R.; Havlicek, M.; Sariciftci, N.; Bouchriha, H. Effect of alkoxy side chains on intra and interchain exciton coupling in PPE-PPV copolymers solution. *Synth. Met.* **2017**, *224*, 72−79.
(50) Guesmi, M.; Fredj, A. B.; Romdhane, S.; Bouguerra, N.; Egbe, D.; Lang, R.; Havlicek, M.; Bouchriha, H. Impact of alkoxy side chains on morphology and excitonic coupling in PPE-PPV copolymer thin films. *J. Lumin.* **2018**, *203*, 447−454.
(51) Yamagata, H.; Spano, F. C. Strong photophysical similarities between conjugated polymers and J-aggregates. *J. Phys. Chem. Lett.* **2014**, *5*, 622−632.

https://doi.org/10.1021/acs.jpcc.4c04825
J. Phys. Chem. C 2024, 128, 16904−16914